9TH INTERNATIONAL SYMPOSIUM ON PARTICLE IMAGE VELOCIMETRY – PIV'11
Kobe, Japan, July 21-23, 2011

Volumetric Measurement of the Transitional Backward Facing Step Flow

J. Kitzhofer[1], C. Brücker[1], O. Pust[2], T. Nonn[2]

[1]Institute of Mechanics and Fluid Dynamics, University of Freiberg, Germany
{jens.kitzhofer,christoph.bruecker}@imfd.tu-freiberg.de

[2]Dantec Dynamics A/S, Skovlunde, Denmark
{oliver.pust,thomas.nonn}@dantecdynamic.com

ABSTRACT

The paper discusses the dynamical behaviour of the Backward Facing Step Flow (BFSF) in the transitional regime at Re_h=4440. The measurements are performed via time resolved 3D Scanning Particle Tracking Velocimetry (3D SPTV) allowing the investigation in a temporal and in a spatial manner. The paper describes main outcomes concerning vortex interactions, i.e. roller and hairpin vortex interaction.

1. INTRODUCTION

Flow Separation (FS) and Flow Reattachment (FR) have been in focus of investigation for more than hundred years since the famous studies of Ludwig Prandtl at the beginning of the 19th century in Göttingen. Understanding the way flow separates and reattaches on a surface is critical in engineering applications.

First studies about separated flows are dated back to 1868 (Helmholtz) and 1869 (Kirchhoff) in case of bluff bodies. From a theoretical, experimental and numerical point of view much effort has been made in understanding the physical background of the flow phenomena. No matter if laminar FS or turbulent FS occurs, the FR is characterized by turbulent flow behaviour. The basic for the analysis of such highly fluctuating flows is the need "to separate the random processes from the non-random processes" as stated by [8]. This statement implies the existence of ordered structures (non-random processes) in turbulence. Via qualitative flow visualization some of the "orderly elements" began "to be recognized and described" as described by [9]. Nevertheless, three-dimensional coherent structures were hidden for quantitative measurements due to insufficient measurement techniques. Here, recent developments in volumetric measurement techniques allow the analysis of the "orderly elements". In fact, results concerning three-dimensional coherent structures in a turbulent boundary layer show the importance for investigation, because these structures seem to form the skeleton of the flow [10]. FS and FR are studied herein in a BFSF. The BFSF is a simplified model of FS and FR as the point of separation is spatially fixed.

2. EXPERIMENTAL SET-UP

The BFSF is studied in a rectangular (50mm x 570mm) closed circuit water channel ($\upsilon=10^{-6}$ m²/s) with canonical channel geometry as sketched in figure 1. The distance between the duct entrance and the volume of interest, called entry length L_E is about 17 time the equivalent diameter $l_{d,eq}$. The channel flow is driven by gravity and the mean flow is regulated via the hydrostatic head. All experiments were carried out for a defined height of the hydrostatic head generating a bulk velocity upstream of the step of U_∞=0.47m/s. The backward facing step is positioned on the bottom of the channel with respect to [1]. The step height h is chosen to 10mm. The length of the ramp as well as the length of the plateau is 60 mm. The aspect ratio AR (B/h) results in 57 and the expansion ratio ER (h_2/h_1) results in 1.25.

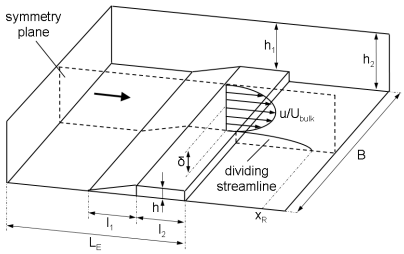

Figure 1 Definition of geometry and major parameters: B =570 mm, L_E=1600 mm, U_{bulk}=0.52 m/s, $l_{d,eq}$=92 mm, l_1=60 mm, l_2=60 mm, h_1=40 mm, h_2=50 mm, h=10 mm, δ=momentum thickness, x_R=reattachment length

An iso-view of the experimental set-up is shown in figure 2. The laser beam of a continuous Argon-Ion laser (8) (Coherent Innova 70, 2 W) passes an optical lens system (9) to adjust the desired thickness of the light sheets. A rotating mirror drum (7) reflects the laser beam into the direction of the measurement volume and generates successively 4 parallel light sheet planes (4). The particle images are recorded with an imaging system consisting of three digital high-speed cameras (Photron APX RS) (3) and telecentric lenses (Sill Optics)(2). The three camera system is installed above the water channel with an angular displacement of about 0°, 45°, -45°. The f-number of the lenses is adjusted to f# = 16 to reach a sufficient depth of focus. A water filled prism reduces astigmatism in the image planes (3). The side of the water channel (10) opposite to the entrance side of the laser is covered with a light absorbing mat that reduces stray reflections, thus giving a black background. The neutrally buoyant seeding particles (6) of roughly 100 µm are injected upstream of the BFS with respect to [1]. The recorded volume is sized to about 90x60x15 mm³.

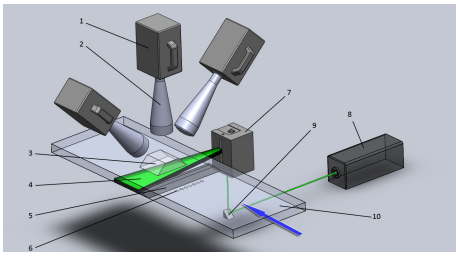

Figure 2. Experimental set-up of backward facing step flow: 1) high speed cameras (3000 fps) 2) telecentric lenses 3) water filled prism 4) voluminous illumination 5) backward facing step 6) seeding injection 7) mirror drum 8) Ar-Ion laser 9) tilted mirror 10) turbulent water channel

3. INLET FLOW CONDITIONS

The inlet flow conditions (bulk velocity, boundary layer thickness, development of velocity profile and sublayer scaled velocity profile) are calculated via 2D Particle Image Velocimetry. Three independently performed planar measurement realizations are used for the calculation of the mean velocity field resulting in a total amount of 12000 vector fields in 480s for statistical independence. The bulk velocity U_{bulk} is calculated at x/h = -0.5 to U_{bulk} = 0.47 m/s, resulting in Reynolds number Re_h based on the step height of 4440 (at 292.15 K). At x/h = -6 the flow exhibits a strong directional change. Here, the boundary layer separates and influences the tunnel flow. A shear layer develops, reattaches and recovers. The length of the recovery region is calculated via the deviation of several velocity profiles between -5<x/h<0.5 from the mean velocity profile at -0.5h. Figure 3 on the left shows the influence of the angled edge, which ranges up to -2h. In the range -2<x/h<0 the deviation is nearly constant. Thus, the flow is considered to have reached a fully developed state again at the backward facing step.

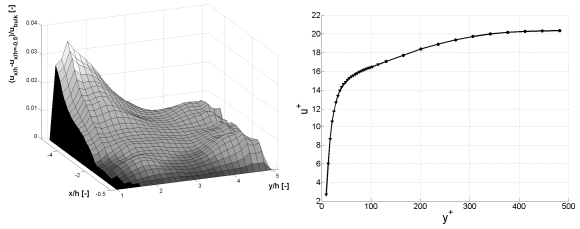

Figure 3. (left) Deviation of several velocity profiles between -5h<x/h<0.5 from the mean velocity profile at -0.5h; **(right)** Sublayer scaled velocity profile in the symmetry plane at x/h = -0.5

The mean velocity profile scaled with the wall shear velocity at y/h = -0.5 is shown in figure 3 on the right. The wall shear velocity u_τ is estimated by the conventional Clauser chart method [2]. The method assumes a universal boundary layer profile. The wall shear velocity u_τ is estimated by a least squares fitting to optimally fit the universal turbulent velocity profile. The wall shear velocity results in $u_\tau = (\tau_W / \rho)^{1/2} = 25$ mm/s $\approx 1/20 U_{bulk}$. The universal constant values used for that purpose are $\kappa = 0.41$ and $A = 5.3$. The scaled velocity profile at x/h = -0.5 clearly indicates a turbulent flow regime.

The normalized boundary layer thickness $\theta^* = \theta/h$ is defined by the momentum thickness with respect to the step height and is calculated to 0.115 at x/h=-0.5.

4. VOLUMETRIC DATA GENERATION

4.1 Velocity field generation

The implemented algorithm for 3D Scanning Particle Tracking Velocimetry is a hybrid PIV/PTV 4-frame method. Hybrid PIV/PTV means that the first guess in which direction a particle has moved is estimated via cross correlation in an interrogation area. 4-frame means that if a particle has been tracked for several time steps, the next position is estimated via the kinematic history of the particle.

For that purpose, the tracking is performed in a single camera view. First, 2D centroid positions of particles are calculated by the gray-value weighted center of area resulting in an uncertainty of 0.02 pix [3]. Next, positions where a particle has moved are estimated by cross correlation or by the kinematic history of a particle. The 3D reconstruction is performed for each two-dimensional trajectory following the inhomogeneous method for stereoscopic point reconstruction [4]. For a given two-dimensional trajectory, homologue particles are searched in the other image planes. For that purpose, the epipolar geometry is applied. The tolerance around the epipolar line is chosen to be 0.5 pix with respect to the uncertainty in 2D centroid estimation. Possible candidates are then reconstructed in three-dimensional space. All particle positions along the trajectory, which can unambiguously be identified, are chosen to be part of the three-dimensional trajectory. The remaining points are studied in a spatio-temporal manner. Here, the temporal length of the pieces of the trajectory characterizes the quality function, nearest neighbour, 3-frame and 4-frame quality function. The three-dimensional position with the smallest deviation from the calculated position is chosen. If the deviation is higher than a certain threshold, the 3D position is not reconstructed resulting in a gap in the trajectory. If a candidate is identified to be part of the trajectory, the three-dimensional point is reconstructed and the corresponding two-dimensional image points are deleted from the database. This is repeated for each two-dimensional trajectory resulting in a dataset consisting of three-dimensional trajectories for each light-sheet. A mean number vector density is calculated to about 42 vectors/cm³.

The post-processing includes the manipulation of the raw trajectories. The manipulation of the raw data is the connecting and smoothing of trajectories and the calculation of velocities and accelerations from the smoothed particle path. The *connection* of trajectories is for two reasons: gaps in the evaluated trajectories due to ambiguities and the use of a scanning illumination.

The identification of homologue trajectories between the light sheets is possible due to the overlapping light sheets. This is done via a simple nearest neighbour criterion in object space as the separation time between the single light sheets is small (1ms) resulting in small particle displacements.

Due to the scanning illumination, the particle positions need to be corrected to represent the same instant in time with equal separation times [5]0. The connection of the trajectories due to gaps, ambiguities or scanning illumination is performed by moving cubic spline interpolation with respect to [6]. The uncertainty in reconstructed 3D position is estimated by analysis of known marker positions resulting in $RMS_{mm,cal}$ = 0.014 mm, which corresponds to $RMS_{pix,cal} \approx 0.16$ pix.

The transformation of the Lagrangian velocity field into the Eulerian velocity field is evaluated by an inverse distance interpolation. Each single time step is interpolated on a grid of 15x90x60 mm³ with 1 mm spacing. In a next step, errorneous vectors are deleted by a simple threshold of magnitude in velocity (0.5 m/s). The resulting velocity field is mean averaged over a 3x3 kernel and further interpolated in a temporal manner by a moving average of three time steps.

4.2 Extraction of shear layer

The extraction of shear layers is a crucial part in the analysis of coherent structures as stated by [7]. Shear layers are formed long before a vortex is born. This is especially true in the case of the BFSF as vortical structures are built due to the shear layer roll up. A simplified approach is used herein, which identifies the shear layer by the analysis of the spatial derivative $\delta u/\delta z$. This is possible due to the geometrical simplicity of the backward facing step as the shear layer is primarily dominated by shear resulting from streamwise velocity gradients perpendicular to the bottom wall, see figure 4 on the left. Thus, the center line of the shear layer is defined by the local maximum of $\delta u/\delta z$ for each x- and y-position. The spatial connection of the single data points into a surface for geometrical representation of the shear layer is performed by a nearest neighbour and intensity criteria. For that purpose, a representative point is chosen as initial guess. The initial guess for the position of the shear layer in region I is $X/h = (0,y,1)^T$.

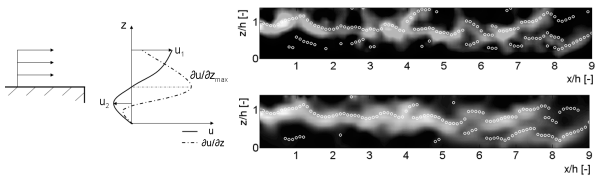

Figure 4. (left) Definition of du/dz_{max}-criterion; **(right)** Comparison of Cr-criterion [7] (upper) and du/dz_{max}-criterion (lower). The plot shows the symmetry plane at y/h=0 and is colour coded by intensity of the single criteria. White means a high intensity and black a low intensity. White dots represent extracted local maxima of the criteria showing the shape of the shear layer.

4.3 Extraction of roller

The *swirling strength criterion* is proposed by [11] for vortex detection. The criterion is an extension of the Δ-criterion by analysing the imaginary part of the eigenvalues resulting in a quantity for the swirling strength and the local plane of swirling.

The three-dimensional center $(x/h, y/h, z/h)^T$ of the vortices in single streamwise symmetry planes is estimated in the following manner. The spanwise position (y/h) is defined by the analyzed plane in y-direction. The height (z/h) and streamwise position (x/h) is estimated via the analysis of the swirling strength value and following analysis of the velocity vector field. For that purpose, each plane coded by the swirling strength criterion is analyzed for local maxima, which are used for a first guess in the vortex center estimation. The exact position results from the w-velocity profile in the vicinity of the local maxima. A characteristic of the developing rollers is that the main axis of rotation is in spanwise direction and that the direction of rotation is clockwise.

The spatial connection of vortex centers to a vortex center line is performed via plane-wise connection of local maxima following the definition that the vortex center line is the connection of plane-wise local maxima with similar properties. Beside the spatial position, properties are e.g. vortex diameter, rotational velocity or rotational direction. The principal is shown in figure 5 on the left and the experimental result is shown in figure 5 on the right. The spanwise displacement of the planes is 0.1h.

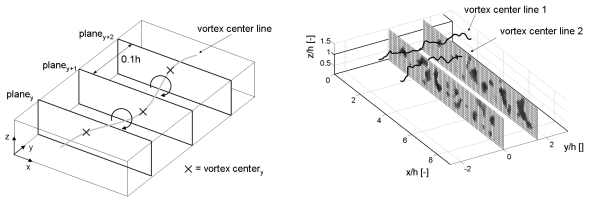

Figure 5. (left) Conceptional reconstruction of a three-dimensional vortex tube (roller) **(right)** Reconstructed vortex center lines. Vortex line in the range 0<x/h<4. Streamwise planes are colour coded by swirling strength

4.4 Extraction of bursts

The measurement inside the recirculation region is rather difficult. The flow is highly three-dimensional and unsteady with a large amount of spatial and temporal length scales. Nevertheless, previous investigations observed vortical structures inside the recirculation region, e.g. hairpin-like vortex structures. While the rollers impinge on the wall, hairpin like vortices are generated in both flow directions. Characteristic of hairpin like vortical structures is the lift-up effect and the corresponding large wall normal velocities at the front of the head and between the legs, thus defining a possible detection criterion. Furthermore, the structures are usually found in vicinity of reattachment, thus the region of interest is located, too.

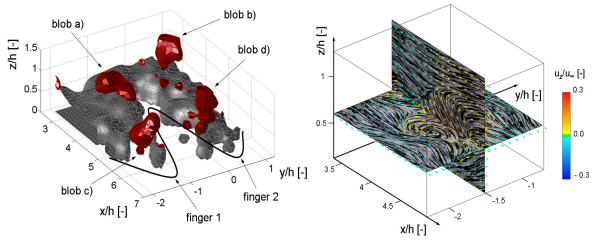

Figure 6. Instantaneous visualization of region of interest positioned about reattachment at t*=27 from figure 4.31 **(left)** gray: iso-surface of zero velocity, red: iso-surface of w/U_∞=0.12; black line: approximated reattachment line **(right)** Blob a) visualized via Line Integral Convolution (LIC) on slices through the hairpin like vortical structure. LIC is superimposed by in plane velocity vectors colour coded by normalized z-velocity

Figure 6 on the left shows the zero velocity iso surface and the +0.12w iso surface of an instantaneous velocity field in the region of interest about reattachment. Four coherent areas of upward directed velocities (blobs) are positioned about reattachment in a certain arrangement. First of all, all blobs are ranging out of the recirculation region, thus interacting with the shear layer and the oncoming rollers. Blob a) and b) are positioned upstream of reattachment and c) and d) are positioned downstream of reattachment. Furthermore, the blobs are aligned in streamwise direction showing a linkage between blobs and reattachment fingers. Figure 6 on the right shows the visualization of an exemplary hairpin vortex and its environment in the inner of the recirculation region (blob a).

5. RESULTS and DISCUSSION

5.1 Roller Formation

Originating from the shear layer instability, coherent vortical structures are formed with major axis of rotation in spanwise direction. Several roll up configurations of the shear layer are identified, i.e. parallel roll up, inclined roll up, convex/concave roll up and piecewise roll up. The most dominant configuration is parallel roll up, but inclined roll ups are observed with inclination angles up to 30° with respect to the step edge, see figure 7 on the right. The Strouhal number for vortex formation is calculated to St_{VS}=0.24. The center line of the roller is identified to be wavy immediately after roller genesis, which generates three-dimensionality immediately downstream of the step. This is postulated to be the result of the wavy shear layer roll up as shown in figure 7 on the left.

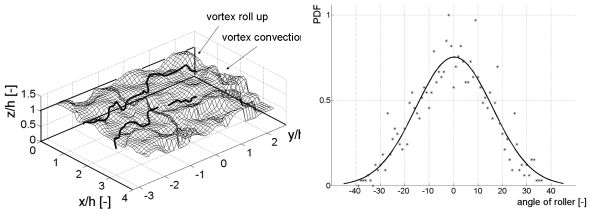

Figure 7. (left) Interaction of shear layer (surface) and vortex center line (black line) in the range 0<x/h<4. **(right)** Probability density function of angle of roller genesis

5.2 Roller Convection

Characteristic of the rollers is the distorted vortex center line. Here, amplitude as well as wave length is estimated. The roller waviness showed distinct specifications depending on the streamwise distance. Thus, the roller performs a stretching in stream-wise direction in between 0<x/h<3. At x/h=3, the roller loops are primarily oriented in stream-wise direction. Further downstream, the rollers perform a tumbling motion resulting in a re-orientation of the loops in a vertical alignment and following tilting to a somehow streamwise alignment.

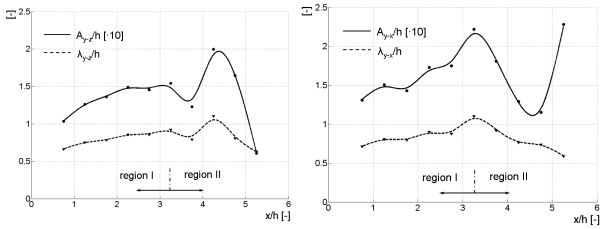

Figure 8. Vortex center line properties as a function of streamwise distance **(left)** properties in y-z-plane **(right)** properties in y-x plane

Reasons for the tumbling motion are found in the pairwise vortex interaction of generated bursts and oncoming rollers as shown in figure 9. The figure on the top shows a measured event, where a burst interacts with an oncoming roller. The schematic representation is shown in figure 9 on the bottom. One identical roller visualized via the vortex center line is tracked for the sequence while influenced by the structure (t_0*≈0, t_1*≈2 t_2*≈4, t_3*≈6, t_4*≈8). The hairpin like structure is visualized via the isosurface of $0.12w/U_\infty$ at t*≈4.5. Furthermore, a slice at z/h=0.1 is colour coded with backward (blue) and forward (white) flow direction identifying the reattachment position at t_4*. The chosen perspective shows the deformation of the roller in vertical direction from t_1* to t_3* while passing over the upward directed velocity. From t_3* to t_4* the vertical aligned vortex loop is reoriented to an inclination angle of roughly 30° with respect to the bottom wall. In between t_2* and t_4*, the distance between vortex and bottom wall is rather large and consequently results in local large amount of backflow generating the backflow finger.

6. CONCLUSION

This article discusses the dynamical and spatial behaviour of the BFSF. In detail, we focus on the generation of the rollers immediately downstream of the step and on the spatial characteristics of the rollers while convecting downstream.

Several roll up configurations of the shear layer are identified, i.e. parallel roll up, inclined roll up, convex/concave roll up and piecewise roll up. The most dominant configuration is parallel roll up, but inclined roll ups are observed with inclination angles up to 30° with respect to the step edge. The Strouhal number for vortex formation is calculated to St_{VS}=0.24. The center line of the roller is identified to be wavy immediately after roller genesis generating three-dimensionality downstream of the step. This is postulated to be the result of the roll up of the wavy shear layer. The roller waviness showed distinct specifications depending on the streamwise distance. A dominant tumbling motion is observed in vicinity of reattachment, which is the result of vortex pair interaction. A roller locally generates larger backflow resulting in a jet directing into the recirculation region. Due to the jet, a hairpin like vortex is born in the inner of the recirculation region. The hairpin vortex interacts with the next oncoming roller and acts as a local bump. The interaction results in a re-orientation of the roller loops from a streamwise alignment in a vertical alignment and following tilting to a somehow streamwise alignment.

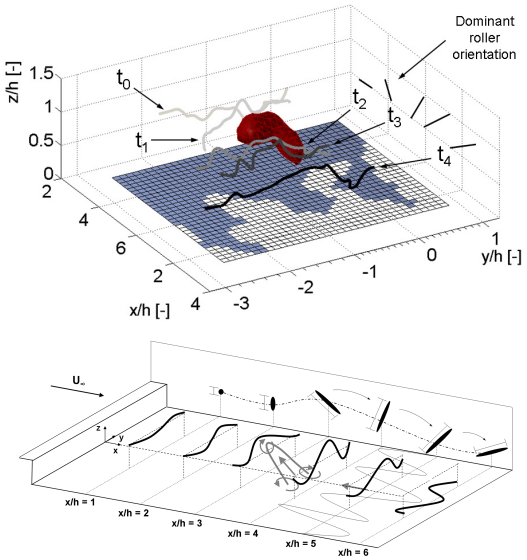

Figure 9. (top) Measured hairpin vortex - roller vortex interaction in the vicinity of reattachment **(bottom)** Schematic of roller development as a function of streamwise distance

REFERENCES

[1] Beaudoin J.-F., Cadot O., Aider J.-L., Wesfreid J.E. (2004) Three-dimensional flow over a backward-facing step. *Europ. Journal of Mechanics B/Fluids* **23**, 147-155.

[2] Clauser F. (1956) The turbulent boundary layer. Adv. ApplMech 4, pp.1.51

[3] Ponitz B., (2010) Experimentelle Untersuchungen der turbulenten Stufenumströmung in einem Wasserkanal mittels drei-dimensionaler optischer Strömungs-messtechnik, Diplom Thesis, TU Freiberg

[4] Schreer O. (2005) Stereoanalyse und Bildsynthese, Springer, Berlin

[5] Hoyer K, Holzner M., Lüthi B., Guala M., Liberzon A., Kinzelbach W. (2005) 3D scanning particle tracking velocimetry Exp. Fluids 29: 145-53

[6] Lüthi B.,Tsinoba A., Kinzelbach W. (2005) *Lagrangian measurement of vorticity dynamics in turbulent flow.* J. Fluid Mech. 528: 87-118

[7] Schafhitzel T., Baysal K., Vaaraniemi M., Rist U., Weiskopf D. (2010) Visualizing the Evolution and Interaction of Vortices and Shear Layers in Time-Dependent 3D Flow. To appear in IEEE Transaction on Visualization and Computer Graphics

[8] Dryden, Hugh L. Recent advances in the mechanics of boundary layer flow. Advances in Applied Mechanics 1, Academic Press, New York, pp.1-40

[9] Roshko A. (1976) Structure of Turbulent shear flows: A new look, AIAA Jpurnal, vol. 14, no. 10, pp. 1349-1357

[10] Schröder A. Geisler R., Staack K., Elsinga G.E., Scarano F., Wieneke B., Henning A., Poelma C., Westerweel J. (2010) Eulerian and Lagrangian views of a turbulent boundary layer flow using time-resolved tomographic PIV. Exp. Fluids 50: 1071-1091 pp.

[11] Zhou J., Adrian R.J., Balachandar S., Kendall T.M. (1999) Mechanism for generating coherent packets of hairpin vortices in channel flow. J. Fluid Mech. 387: pp. 353-396